RANS MODELING FOR FLOWS ON RIBLETS BASED ON EXPERIMENTAL DATA

Kie OKABAYASHI*, Takanori MATSUE, Masahito ASAI** and Hiroshi NAITO***
***Japan Aerospace Exploration Agency, **Department of Aerospace Engineering, Tokyo Metropolitan University**
Keywords: *Riblet, Drag reduction, RANS, Computational Fluid Dynamics*

Abstract

For practical CFD-aided design of riblets on aircraft, we are aiming to develop a Reynolds-Averaged Navier-Stokes (RANS) turbulence model which can simulate drag reduction effects without resolving fine-scale secondary flows near the riblets. Wilcox's rough wall boundary conditions for Menter's SST model are modified in order to reproduce velocity shift in the logarithmic region corresponding to riblet's drag reduction effects. Two basic relations for this model are derived from experimental results and parametric analysis, and are validated on two different-geometry riblets. As a result, it is confirmed that drag reduction rates comparable to the experimental results for two riblet's geometries can be obtained respectively with the two relations.

1 Introduction

Attention must be paid for sustainable aviation to improve the fuel efficiency aiming at the reduction of CO2 emission. Reduction of skin friction drag will contribute significantly to improve aerodynamic performance: friction drag accounts for about half of total drag of aircraft at cruising condition. Recently several research groups have focused renewed attention on riblet as a realizable flow control device [1]. Riblets are rows of many fine-scale grooves which are arranged in the streamwise direction (e.g. Fig. 1.1). and was developed at NASA Langley Research Center in the late 70's. Two-percent reduction of total air drag was confirmed by the Airbus A320 flight test, which corresponds to an annual saving of more than

Fig. 1.1 Riblet surface of 3M company [1].

50000 litters fuel consumption per aircraft in normal regular service [2]. As for CFD-aided design of riblets on aircraft, it is essential to estimate drag reduction rates all over the surface of the aircrafts. Fine-scale computations such as Direct Numerical Simulation (DNS) and Large-Eddy Simulation (LES) are difficult to be conducted for this subject because of their huge computational cost, though they can resolve the flow over riblets and show the detailed physical phenomena. For practical use, therefore, we are aiming to develop a Reynolds-Averaged Navier-Stokes (RANS) turbulence model which enables us to simulate drag reducing effects without reproducing fine-scale secondary flows near the riblets.

2 Background of model

On the smooth surface, the standard logarithmic law is

$$u^+ = \frac{1}{\kappa} log(y^+) + C \qquad (2.1),$$

where κ denotes the von Kármán constant $\kappa \approx 0.41$ and C=5.0. On the rough surface, on the other hand, eq. (2.1) is altered, with a velocity shift ΔU^+, as

$$u^+ = \frac{1}{\kappa} log(y^+) + C + \Delta U^+ \qquad (2.2).$$

The velocity shift ΔU^+ is negative when drag is increased [3-5] and positive when reduced [5]. Tani [5] reported that this relation on rough wall can be applied to that on the riblet surface. Therefore, the velocity shift ΔU^+ characterizes a drag reduction effect of riblet. In previous researches by Aupoix et al. [6] and Mele & Tognaccini [7], they introduce riblets' drag reducing effects to RANS models: basically they modify baseline models such as Spalart-Allmaras turbulence model [8] or SST turbulence model [9] to reproduce the velocity shift ΔU^+ corresponding to drag reducing effects of riblets. Although the fine-scale secondary motion over the riblet isn't reproduced, via ΔU^+ these models can estimate drag reduction rates which are determined by configuration, spacing and height of riblet as well as orientation to the near-wall flow direction. Starting from this idea, we propose a new model by employing the existing experimental data, and validate the computational results.

3 Modeling

Wilcox [10] altered the wall boundary condition of Menter's SST $k-\omega$ model [9] as follows to estimate friction drag on rough wall:

$$\omega = \frac{{u_\tau}^2}{\nu} S_R({k_s}^+) \qquad (3.1)$$

$$S_R = (50/k_s^+)^2 \quad (k_s^+ < 25) \qquad (3.2)$$

$$S_R = 100/k_s^+ \quad (k_s^+ \geq 25) \qquad (3.3)$$

where u_τ denotes the wall friction velocity, ν the kinematic viscosity, S_R the wall roughness function and ${k_s}^+$ the Reynolds number based on the roughness height.

In this study, we modify the wall function S_R to fit ΔU^+ to the corresponding riblets' experimental data. Riblets' drag reduction rates are determined by riblets' configuration, spacing, height and orientation to the near-wall flow direction, so the modified function S_R must include those properties as parameters. Our modeling process is the following:

1. Obtain the function $\Delta U^+ = f_1(\Delta C_f)$ (ΔC_f: drag reduction rates) from the experiment by Sawyer & Winter[11] and Gaudet[12]. Drag reduction rates ΔC_f is defined as

$$\Delta C_f = \frac{D_{riblet} - D_{smooth}}{D_{smooth}} \qquad (3.4)$$

where D_{riblet} and D_{smooth} represent the friction drag on riblet and smooth surface, respectively.

2. Conduct a parametric analysis about S_R (just a parameter in this step, i.e. unformulated) and obtain the function $S_R = f_2(\Delta U^+)$ by curve fitting.
3. Obtain relations between h^+ (wall-unit of riblet height) and ΔC_f, which are called the drag reduction rate curves later, from a number of experimental results.
4. Input the above relation to $\Delta U^+ = f_1(\Delta C_f)$ and obtain a function $\Delta U^+ = f_3(h^+)$ by curve fitting.
5. Input the function $\Delta U^+ = f_3(h^+)$ to $S_R = f_2(\Delta U^+)$ and derive the wall function $S_R(h^+)$.
6. Calculate the drag reduction rate by using the new model and validate the results.

As mentioned above, this model is based on the existing experimental data: the relation between ΔU^+ and ΔC_f from ref. [11,12] (step 1), and as many "drag reduction rate curves" as possible from many experiments (step 3). Particularly, ΔU^+ was measured only by Sawyer & Winter [11] and Gaudet [12].

This model is inspired by the following ideas:

(a) In previous researches, they modified the baseline RANS model to reproduce the velocity shift ΔU^+ corresponding to the drag reducing effects of riblets.

(b) Every wall roughness can be converted "equivalent sand roughness", which is defined as the surface roughness uniformly covered with spheres of diameter ${k_s}^+$ (${k_s}^+$: equivalent sand roughness height), and gives the same ΔU^+ as the corresponding wall roughness [3,4]. In addition, the equivalent sand roughness is uniquely related to ΔU^+, or the friction drag coefficient [4]. Therefore, we expect that the drag reduction rate ΔC_f is represented with ΔU^+, in the same manner as the relation between sand roughness and ΔU^+.

(c) We also expect that a number of existing experimental results, i.e. drag reduction rate curves (relations between ΔC_f and h^+ or s^+(wall-unit of spacing)), can be employed as database for the modeling.

A characteristic feature of this model is that the velocity shift ΔU^+ is estimated by the drag reduction rate ΔC_f which is obtained from the experimental results of Sawyer & Winter [11] and Gaudet [12], as mentioned in (b).

3.1 Relation between velocity shift ΔU^+ and drag reduction rate ΔC_f (step 1)

Sawyer & Winter [11] conducted experiments to obtain relations between ΔC_f and h^+ (or s^+). Fig. 3.1 shows the riblets' configurations adopted in their experiments. Fig. 3.2 represents drag reduction rate curves for various h^+ [11]. The velocity shift ΔU^+ for various h^+ (or s^+) was also measured by Gaudet [12] (Fig. 3.3). We adopt these data; there are few experiments concerning ΔU^+ over the riblet. As for the corresponding values of s^+, see [11,12].

Fig. 3.4 represents a relation between ΔC_f and ΔU^+ which is derived from Fig. 3.2, 3.3. From the experimental results, it is clearly shown that the relation between ΔC_f and ΔU^+ is linear. Therefore, from the experimental results, we estimate a linear relation

$$\Delta U^+ = -13.25\Delta C_f + 0.1813 \quad (3.5).$$

By the least square method (black line in Fig. 3.4). Although a little intercept, which may be

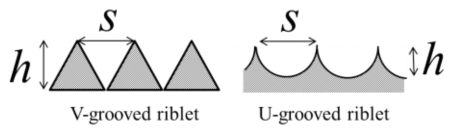

Fig. 3.1. Riblets' configuration adopted in experiments by Sawyer & Winter [11] and Gaudet [12]

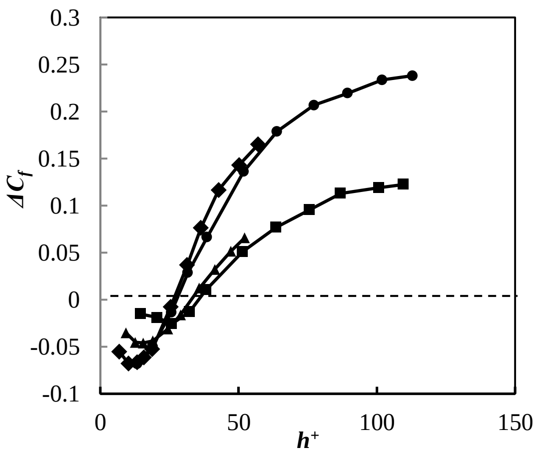

Fig. 3.2. Drag reduction rate ΔC_f for various h^+ (Sawyer & Winter [11]).

◆ : V-grooved, s/h=1.28,
■ : V-grooved, s/h=2.08,
▲ : U-grooved, s/h=2.50,
● : U-grooved, s/h=2.20

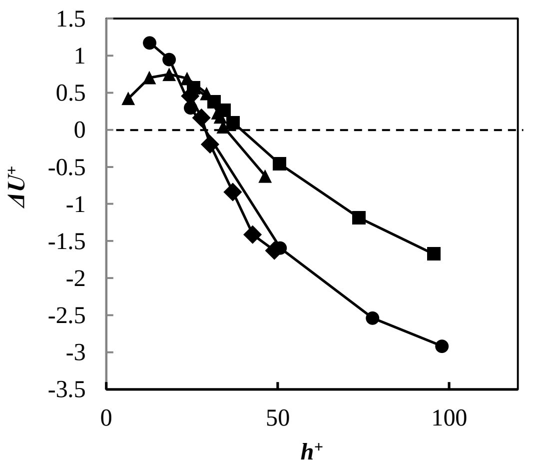

Fig. 3.3. Velocity shift ΔU^+ for various riblet heights h^+(Gaudet [12]).

◆ : V-grooved, s/h=1.28,
■ : V-grooved, s/h=2.08
▲ : U-grooved, s/h=2.50,
● : U-grooved, s/h=2.20

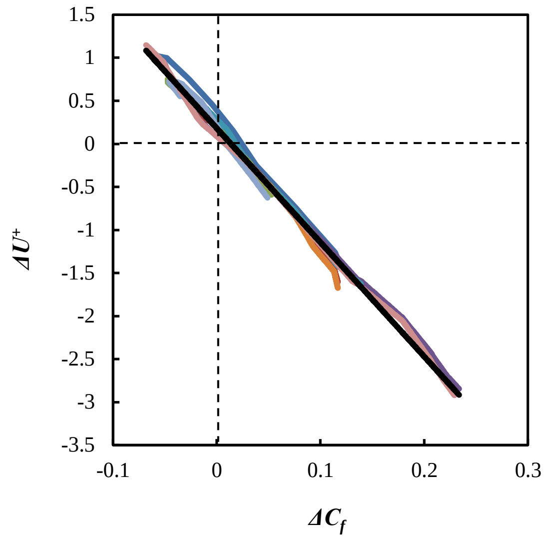

Fig. 3.4. Relation between ΔC_f and ΔU^++.

◆: V-grooved (via h+), s/h=1.28,
■: V-grooved (via h+), s/h=2.08,
▲: U-grooved (via h+), s/h=2.50,
✕:U-grooved (via h+), s/h=2.20,
●: V-grooved (via s+), s/h=1.28,
✻: V-grooved (via s+), s/h=2.08,
+: U-grooved (via s+), s/h=2.50,
-: U-grooved (via s+), s/h=2.20,
—: Eq. (3.5)

caused by errors of measurement or reading data, is left, we can confirm that ΔU^+ is positive when friction drag is reduced ($\Delta C_f < 0$), and negative when friction drag is increased ($\Delta C_f > 0$).

3.2 Relation between model function S_R and velocity shift ΔU^+ (step 2)

In this step a parametric analysis about the model function S_R (just a parameter in this step) is conducted to obtain the relation between S_R and ΔU^+.

3.2.1 Analysis object

Analysis is conducted for flat-plate turbulent boundary layer. Flow conditions are Mach number $M = 0.1$ and unit Reynolds number $Re = 1.0 \times 10^6$ [1/m]. Computational domain and boundary conditions are shown in Fig. 3.5. Here, Resource of NASA Langley Research Center [13] is refered for turbulence Modeling.

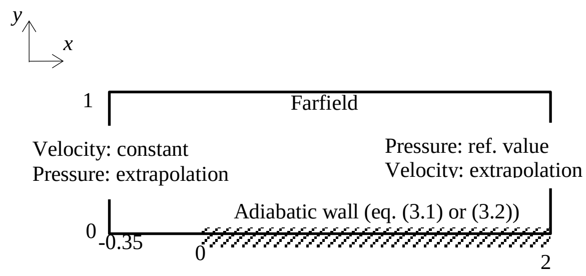

Fig. 3.5. Computational domain and boundary conditions of flat-plate turbulent boundary layer.

Adiabatic wall is employed at $y = 0$ and $0 \leq x \leq 2$. At the wall, eq. (3.1) is applied as ω boundary condition. As the reference smooth surface, eq. (3.2) of ${k_s}^+ = 4$ is applied [4]. Numbers of Grid are 273, 193 and 1 for rhe x, y and z directions, respectively. At the vicinity of $x = 0$ and $y = 0$, cells are finer to get high resolution. Particularly in the y-direction, the first cell on the wall is set within the viscous sublayer. Symmetric wall boundary condition is imposed in the z-direction.

3.2.2 Numerical method & validation

The governing equation is Reynolds-Averaged Navier-Stokes equation. We use the fast unstructured CFD code “FaSTAR” developed in JAXA [14].

Menter’s SST turbulence model [9] is employed as turbulence model. Discretization is cell-centered finite volume method. As inviscid flux, HLLEW [15] which is improved based on HLLE proposed by Einfeld is used. The gradients are computed with weighted Green-Gauss. Gradient limiter is Hishida’s limiter of van Leer type [16]. Time integration is LU-SGS by local time stepping [17].

Before conducting parametric analysis about S_R in step 2 and computing ΔC_f later (in step 6), the computational setup mentioned above is validated by comparing the velocity profile and local friction drag coefficient $C_{f_{local}}$. Here, we employed the wall boundary condition

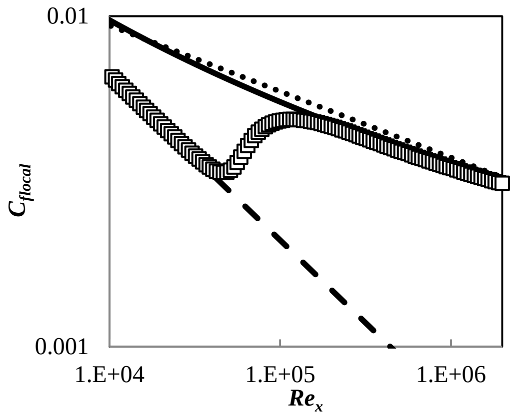

Fig. 3.6. Local friction drag coefficient $C_{f_{local}}$ versus Re_x.
dot: 1/7 power law (eq. (3.7) [18]), solid: Karman-Schoenherr eqation (eq. (3.8)[19]), dash: Blasius' drag law for laminar flow (eq. (3.10)[4]), □: computed value.

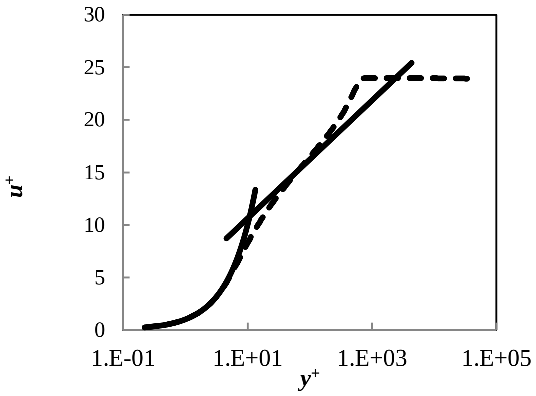

Fig. 3.7. Velocity profile ($Re_x = 0.95 \times 10^6$) compared with law of wall.
dash: computed value, solid: law of wall.

$$\omega = \frac{6\nu}{\beta y^2} \quad (3.6)$$

which is generally used as the wall boundary condition of Menter's SST turbulence model [9].

Fig. 3.6 displays computed local friction drag coefficient $C_{f_{local}}$ against Re_x. For comparison, theoretical curves derived from the 1/7 power law with correction by the experimental value [18]

$$C_{f_{local}} = \frac{0.0592}{{Re_x}^{1/5}} \quad (3.7),$$

Karman-Schoenherr equation with theoretical value of Reynolds number based on momentum thickness [19]

$$C_{f_{local}} = \frac{0.0586}{[\log_{10} 2Re_\theta]^2 + 0.8686 \log_{10} 2Re_\theta} \quad (3.8),$$

$$Re_\theta = 0.036{Re_x}^{0.8} \quad (3.9),$$

and, Blasius' drag law for laminar flow [4]

$$C_{f_{local}} = \frac{0.664}{{Re_x}^{1/2}} \quad (3.10)$$

are also shown in Fig. 3.6. It is confirmed that $C_{f_{local}}$ computed have a good agreement with the theoretical values both before and after transition. Fig. 3.7 displays computed velocity profile at $Re_x = 0.95 \times 10^6$, where turbulent flow is fully developed. The u^+ profile also shows good agreement with the law of wall.

3.2.3 Parametric analysis

Fig. 3.8 displays an example of velocity profiles at $Re_x = 0.95 \times 10^6$ in the fully developed region for parametrically-changed S_R. Here, S_R is set at 10^1, 10^2, 10^3, 10^5, 10^7, 10^9, 10^{11}, 10^{13}, 10^{15} and 10^{17}. Solid line represents the corresponding velocity profile over smooth surface. The figure shows that the velocity u^+ gets larger in both logarithmic and wake regions with larger S_R. From these profiles, the velocity shift ΔU^+ for each given S_R is calculated and shown in Fig. 3.9. Here, ΔU^+ is calculated as a deviation from velocity profiles over smooth surface. Three markers in Fig. 3.9 represent ΔU^+ in the fully-developed region i.e., at $Re_x = 0.50 \times 10^6$, 0.95×10^6 and 1.95×10^6, respectively. From this figure, it is presumed that almost the same ΔU^+ is obtained with respect to the same S_R even though the locations (Re_x) are different: note that velocity profiles themselves are different for different Re_x. Fitting curve

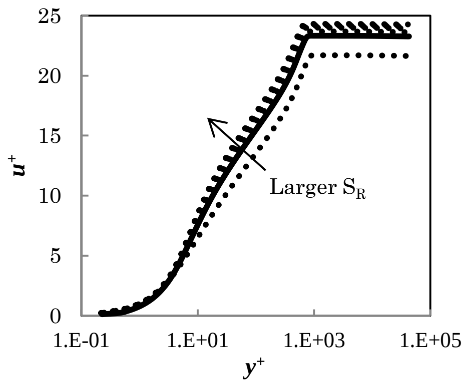

Fig. 3.8. Velocity profile for various model function S_R at $Re_x = 0.95 \times 10^6$.
solid: smooth, dot: riblet

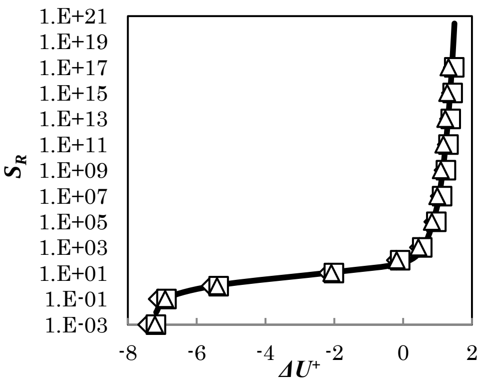

Fig. 3.9. Velocity shift ΔU^+ versus various model function S_R.
◇: $Re_x = 0.50 \times 10^6$,
□: $Re_x = 0.95 \times 10^6$,
△: $Re_x = 1.95 \times 10^6$,
—: eq. (3.11)

$$\log_{10} S_R = 3 \times 10^{-3} \times (\Delta U^+ + 3.25)^{13} + 0.3 \times \Delta U^+ + 1.7 \quad (3.11),$$

is obtained, by trial and error, as the relation between S_R and ΔU^+. Equation (3.11) is also shown in Fig. 3.9.

3.3 Relation between riblet height h^+ and velocity shift ΔU^+ (step 3, 4)

A number of drag reduction rate curves (relations between ΔC_f and h^+ or s^+) were obtained from the past experiments. In this study, we substitute above relation to

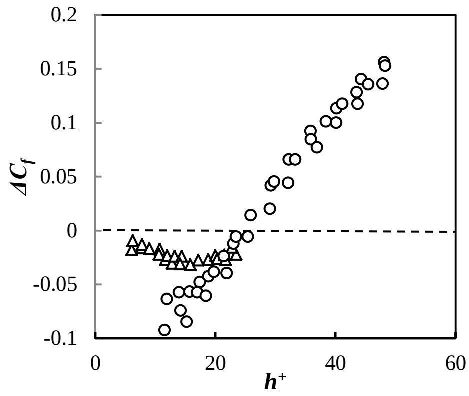

(a) Walsh(1982), s/h=1 [16]
△: s=0.25mm, ○: s=0.52mm

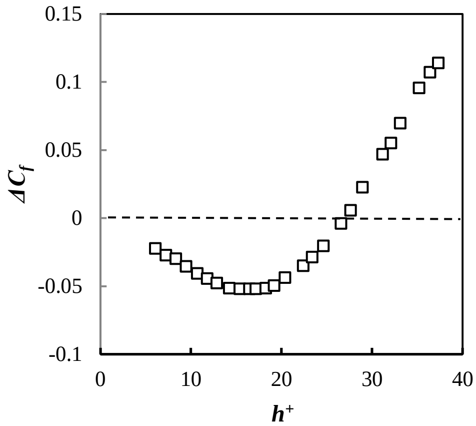

(b) Bechert (1997), s/h=0.86 [22]

Fig. 3.10. Drag reduction curves (riblet height h^+ versus Drag reduction rate ΔC_f) from experiment by Walsh [19] and Bechert [22].

$\Delta U^+ = f_1(\Delta C_f)$, *i.e.* eq. (3.5) and obtain the relation $\Delta U^+ = f_3(h^+)$ by curve fitting. At this step, effects of riblet's misalignment against the near-wall flow direction [20-22] can be considered if the yaw angle is related to the necessary parameter. We use the drag reduction rate curves of Walsh [19] and Bechert et al. [23] (Fig. 3.10 (a), (b)) to eq. (3.5). Each velocity shift ΔU^+ estimated as the output of eq. (3.5) is shown in Fig. 3.11 (a) and (b), respectively. Fitting curves passing through (0, 0) are obtained:

$$\Delta U^+ = (5.00 \times 10^{-5}) h^{+3} + 0.0052 h^{+2} + 0.105 h^+ \quad (3.12)$$

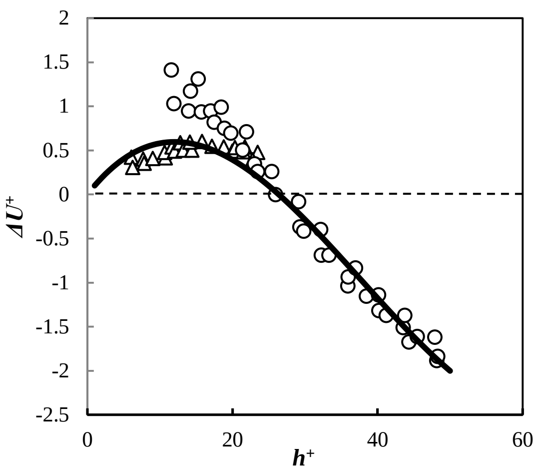

(a) Walsh(1982), s/h=1 [19]
△, ○: Estimated ΔU^+ (experimental result plotted in Fig. 3.10 (a) is assigned to eq. (3.5)), —: eq. (3.12)

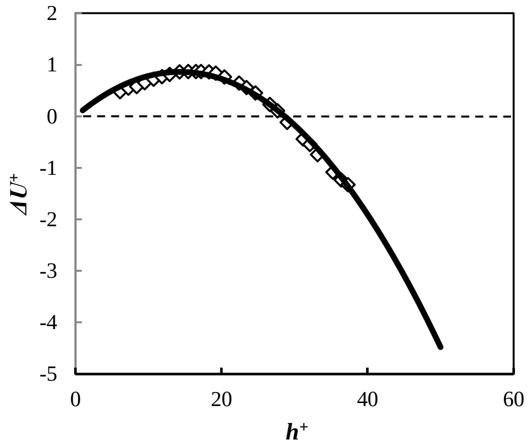

(b) Becher t (1997), s/h=0.86 [23]
◇: Estimated ΔU^+ (experimental result plotted in Fig. 3.10 (b) is assigned to eq. (3.5)), —: eq. (3.13)

Fig. 3.11. Relation between riblet height h^+ and velocity shift ΔU^+.

for Walsh's riblet [19] and

$$\Delta U^+ = -0.00042{h^+}^2 + 0.1204h^+ \qquad (3.13)$$

for Bechert et al.'s riblet [23]. These equations give $\Delta U^+ = f_3(h^+)$. The relation between h^+ and ΔU^+. Equations (3.12) and (3.13) are also plotted in Fig. 3.11(a) and (b), respectively.

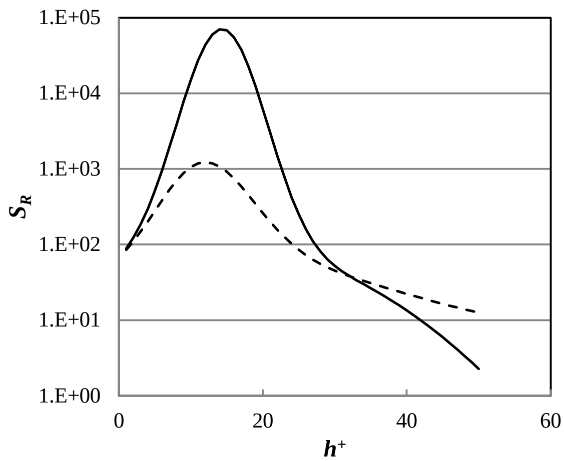

Fig. 3.12. New model function $S_R(h^+)$. dash: Walsh [19], solid: Bechert et al. [23]

3.4 Deriviation of new model function $S_R(h^+)$ (step 5)

In this step, we substitute $\Delta U^+ = f_3(h^+)$ (eq. (3.12) or eq. (3.13)) to $S_R = f_2(\Delta U^+)$ (eq. (3.11)), and derive a new model function $S_R(h^+)$.
The model functions of $S_R(h^+)$ derived for Walsh's riblet [19] and Bechert et al.'s riblet [23] are shown in Fig. 3.12.

4 Validation (step 6)

Finally, the parametric analysis about h^+ is conducted to validate the new model function $S_R(h^+)$ obtained in step 5. The target flow, computational condition and numerical method are the same as those in step 2, except $S_R(h^+)$. Local drag reduction rates $\Delta C_{f_{local}}$ at $Re_x = 0.5\times10^6$, 1.0×10^6, 1.5×10^6, and 2.0×10^6 are obtained from the local friction drag coefficient $C_{f_{local}}$. Also, drag reduction rate ΔC_f is obtained from the friction drag coefficient C_f, which is computed from the surface integral of $C_{f_{local}}$ from $Re_x = 0.2\times10^6$ to 2.0×10^6. $\Delta C_{f_{local}}$ at each location and ΔC_f are shown in Fig. 4.1 with the corresponding experimental results.

It is clear that the computed drag reduction rates are in good agreement with the experimental results. This result indicates that

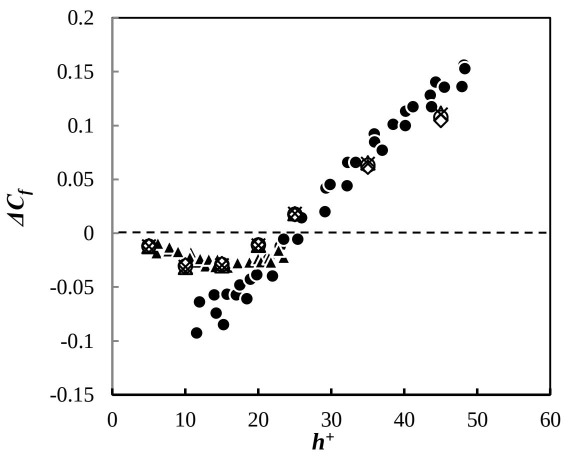

(a) Walsh(1982), s/h=1 [19]
□: $Re_x = 0.5 \times 10^6$,
△: $Re_x = 1.0 \times 10^6$,
○: $Re_x = 1.5 \times 10^6$,
◇: $Re_x = 2.0 \times 10^6$,
×: integral (from $Re_x = 0.2 \times 10^6$ to 2.0×10^6),
▲: experiment (s=0.25mm),
●: experiment (s=0.52mm)

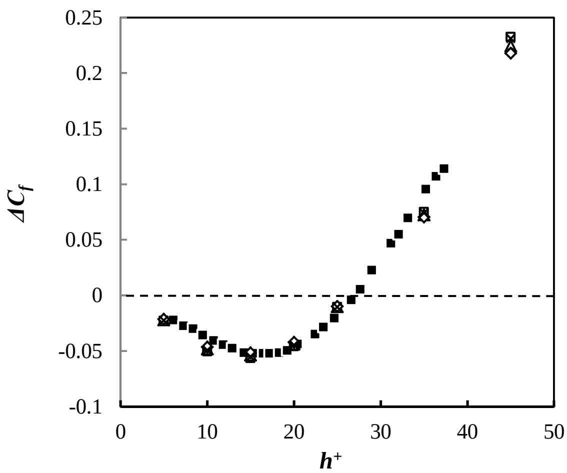

(b) Bechert(1997), s/h=0.86 [23]
□: $Re_x = 0.5 \times 10^6$,
△: $Re_x = 1.0 \times 10^6$,
○: $Re_x = 1.5 \times 10^6$,
◇: $Re_x = 2.0 \times 10^6$,
×: integral (from $Re_x = 0.2 \times 10^6$ to 2.0×10^6),
■: experiment

Fig. 4.1. Drag reduction rate ΔC_f computed by using new model.

eq. (3.5) and (3.11), which are the basis of our new model, work well.

References

[1] Stenzel, V., Wilke, Y., Hage, W, Drag-reducing Paints for the Reduction of Fuel Consumption in Aviation and Shipping, Progress in Organic Coating, Vol. 70, pp. 224-229, 2011.

[2] MBB Transport Aircraft Group, Microscopic Rib Profiles Will Increase Aircraft Economy in Flight, Aircraft Engineering, Vol. 60, No. 1, pp. 11, 1988.

[3] Jimenez, J., Turbulent Flows over Rough Walls, Annu. Rev. Fluid Mech., Vol. 36, pp. 173-196, 2004.

[4] Schlichting, H. and Gersten, K., Boundary Layer Theory, 8th Revised and Enlarged Edition, Springer , pp. 159, 2000.

[5] Tani, I., Drag Reduction by Riblet Viewed as Roughness Problem, Proc. Japan Acad., Vol. 64 Ser. B, pp. 21-24, 1988.

[6] Aupoix, B., Pailhas, G. and Houdeville, R., Towards a General Strategy to Model Riblet Effects, AIAA Journal, Vol. 50, No. 3, pp. 708-716, 2012.

[7] Mele, B. and Tognaccini, R., Numerical Simulation of Riblets on Airfoils and Wings, 50th AIAA Aerospace Sciences Meeting including the New Horizons Forum and Aerospace Exposition, AIAA2012-0861, pp. 1-16, 2012.

[8] Spalart, P. and Allmaras, S., A One-equation Turbulence Model for Aerodynamic Flows, AIAA Paper, 1992-0439, 1992.

[9] Menter, F. R., Kuntz, M. and Langtry, R., Ten Years of Industrial Experience with the SST Turbulent Model, Turbulence, Heat and Mass Transfer, ed. Hanjalic, K., Nagano, Y. and Tummers, M., pp. 625-632, 2003.

[10] Wilcox, D. C., Turbulence Modeling for CFD, second edition, DCW Industries (1998).

[11] Sawyer, W. and Winter, K., An Investigation of the Effect on Turbulent Skin Friction of Surface with Streamwise Grooves, Turbulent Drag Reduction by

Passive Means, The Royal Aeronautical Society, pp. 330-362, 1987.
[12] Gaudet, L., An Assessment of the Drag Reduction Properties of Riblets and the Penalties of Off-Design Conditions, Turbulent Drag Reduction by Passive Means, The Royal Aeronautical Society, pp. 363-376, 1987.
[13] http://turbmodels.larc.nasa.gov/flatplate.html
[14] Hashimoto, A., Murakami, K., Aoyama, T., Ishiko, K., Hishida, M., Sakashita, M. and Lahur, P. R., Toward the Fastest Unstructured CFD Code "FaSTAR", Proc. of 50th AIAA Aerospace Sciences Meeting including the New Horizons Forum and Aerospace Exposition, AIAA 2012-1075 (2012).
[15] Obayashi, S. and Guruswamy, G. P., Convergence Acceleration of a Navier-Stokes Solver for Efficient Static Aeroelastic Computations, AIAA J., Vol. 33, No. 6, pp. 1134-1141, 1995.
[16] Hishida, M., Hashimoto, A., Murakami, K. and Aoyama, T., A new slope limiter for fast unstructured CFD solver FaSTAR, Proc. of 42nd Fluid Dynamics Conference / Aerospace Numerical Simulation Symp. 2010 (in Japanese), 1C10, 2010.
[17] Sharov, D. and Nakahashi, K., Reordering of Hybrid Unstructured Grids for Lower-Upper Gauss-Seidel Computations, AIAA J., Vol. 36, No. 3, pp. 484-486, 1998.
[18] http://www.desktop.aero/appliedaero/blayers/turbbl.html
[19] Walsh, M. J., Turbulent Boundary Layer Drag Reduction Using Riblets, AIAA Paper, 82-0169, 1982.
[20] Gaudet, L., Properties of Riblets at Supersonic Speed, Appl. Sci. Res., Vol. 46, pp. 245-254, 1989.
[21] Hage, W., Bechert, D. W. and Bruse, M., Yaw Angle Effects on Optimized Riblets, Aerodynamic Drag Reduction Technologies: Proceedings of the CEAS/DragNet European Drag Reduction Conference, pp. 278-285, 2000.
[22] Coustols, E. and Savill, A. M., Turbulent Skin-friction Drag Reduction by Active and Passive Means: Part 1, Defense Technical Information Center Document, pp. 1-53, 1992.
[23] Bechert, D. W., Bruse, M., Hage, W., van der Hoeven, J. G. T. and Hoppe, G., Experiments on Drag-reducing Surfaces and their Optimization with an Adjustable Geometry, J.Fluid Mech, Vol.338, pp. 59-87, 1997.

Contact Author Email Address

mailto:okabayashi.kie@jaxa.jp

Acknowledgement

This research was supported by Numerical Simulation Research Group (NSRG) of JAXA for the use of the numerical code 'FaSTAR.'

Copyright Statement